To Mix or Not to Mix: Charge and Polarity Effects on Alkyl/Fluoroalkyl Compound Miscibility

Joshua Lai[a], Evelyn F. Gladden-Bennett[a], Karina Shimizu*[b], Naomi S. Elstone[a], Theo F. N. Tanner[a], Bruno Demé[c], Adrian C. Whitwood[a], Seishi Shimizu[a], Jose N. Canongia Lopes[b], John M. Slattery*[a] and Duncan W. Bruce*[a]

Supporting Information

Experimental

All materials were prepared in house with details given in the SI. ^{1}H and $^{13}C\{^{1}H\}$ NMR spectra were recorded on a Jeol ECS400 spectrometer operating at 400 MHz, with chemical shifts referenced to appropriate residual non-deuterated solvent signal.

Elemental analysis (CHN) was carried out by Dr Scott Hicks on an Exeter Analytical Inc. CE-440 analyser.

Differential scanning calorimetry was recorded on a Mettler DSC 822^{e} calibrated using an indium standard (onset = 156.55 ± 0.2 °C, ΔH = 28.45 ± 0.40 J g^{-1}) and a scan rate of 5 °C min^{-1}, operated using Mettler STAR-E software, under an atmosphere of dry dinitrogen.

Surface Tension

Measurements were collected using the pendant drop method using a Dataphysics OCA 25, equipped with a syringe heating device SHD as well as a Peltier temperature control unit TPC 160, with liquid counter cooling and TC 160Pro PID controller. The software used to acquire values for Interfacial Tension (IFT) from the collected images was SCA20. Measurements for compositions where $0.1 \leq x \leq 1$ were taken at 55 ± 0.1 °C, where the sensor was adjacent to the drop being measured. ImC_8-F_{13} required use of a slightly elevated temperature due to having a higher melting point, and a range of 58.3 – 58.6 °C was used to obtain these measurements. The measurements employed Dataphysics flat-ended needles with an outer diameter of 0.91 mm and inner diameter of 0.61 mm, which was used as the reference size for the measurements. The densities of the mixtures were calculated as described previously. Each measurement was taken between 4-6 times then the results were averaged and standard error was calculated using Equation 3.

$$\Delta x = \frac{\sigma}{\sqrt{n}} \qquad where:\ \sigma = \sqrt{\frac{1}{n-1}\sum_{i=1}^{n}(x_i - \bar{x})^2} \qquad (1)$$

and where Δx is the standard error in the mean, σ is the estimated standard deviation, $\bar{x}$ is the average over n number of measurements, and x_i is each measurement value.

Surface tension is a linear function of density and so we have allowed for the fact that the surface tension measurements were made some 35 °C higher than the density measurements by correcting using the volumetric expansion coefficients for octane of ≈10^{-3} g cm^3 K^{-1} and for perfluorooctane of *ca* 4 x 10^{-4} cm^3 K^{-1} (taken as reasonable proxies for C_8Im and C_8Im-F_{13}, respectively).

Values of the surface tension at 296 K for C_8Im and C_8Im-F_{13} were estimated from the higher-temperature experimental data according to data found in Kou *et al.*[1]

SAXS Measurements

Small-angle X-ray scattering (SAXS) employed a Bruker D8 Discover diffractometer equipped with a bespoke temperature-controlled, bored-graphite rod furnace, custom built at the University of York. Cu-K_α (λ = 0.154056 nm) radiation was used, generated from a 1 mS microfocus source. Diffraction patterns were recorded on a 2048 x 2048-pixel Bruker VANTEC 500 area detector set at a distance of 106.5 mm from the sample, allowing simultaneous collection of small- and wide-angle scattering data. Mixtures used employed only hydrogenous components.

SANS Measurements

Raw data are found at: https://doi.ill.fr/10.5291/ILL-DATA.9-12-720.

Small-angle neutron scattering (SANS) measurements were carried out at the Institut Laué Langevin (ILL, Grenoble, France) on the recently upgraded D16 instrument, a cold neutron diffractometer, which uses a highly orientated pyrolytic graphite (HOPG) monochromator to focus the beam along the vertical axis. Set to a take-off angle of 85°. This gave access to a neutron wavelength of 4.47 Å. The nine crystals which make up the monochromator are orientated to maximise the incident neutron flux by focusing the beam to the sample. The desired *q*-range (0.015 - 1.1 $Å^{-1}$) was obtained in a single detector position via the new curved 2D MWPC ^{3}He detector developed at the ILL in the frame of the instrument upgrade.[2] Samples were measured in 1 mm path length and 1 cm wide quartz cuvettes. The data were corrected for the sample container and instrument background, normalised to water and reduced to 1D using Mantid.[3]

SAXS and SANS Fitting

Fitting of the SAXS and SANS data was carried out with SasView, using a combination of Lorentzian functions to describe peaks and a spherical form factor to describe the low-*q* scattering from small scattering objects. For the sphere model (see below),[4] in order to minimise the number of variables in the fits, a fixed SLD difference between the sphere and solvent of 3 x 10^{-6} $Å^{-2}$ was used and the scale factor (volume fraction) was varied. The sphere radius was initially set at 10 Å, based on the SANS data where x = 0.2 to 0.5 and the radius is more clearly defined, and held constant while other parameters were varied in the fits, before being allowed to refine. In addition to the CP (q ~ 1.3 $Å^{-1}$) and PNPP (q ~ 0.3 $Å^{-1}$) low-intensity scattering in between these was seen for many samples (See Figs. S1 and S2 below). The physical significance of this low-intensity scattering is not clear and as such we have not attempted to interpret it. However, in order to ensure the best fitting of the positions and intensities for the other peaks and the low-*q* scattering, a broad Lorentzian function around q = 0.5 was included in most fits to account for scattering in this intermediate region. Its

position was varied by hand during fitting to best describe the data and its width was allowed to freely vary with the fit.

$$\textbf{\textit{Sphere Model}}: I(q) = \frac{\text{scale}}{V} \bullet \left[3V(\Delta\rho) \bullet \frac{\sin(qr) - qr\cos(qr)}{(qr)^3}\right]^2 + \text{background}$$

Where *scale* is a volume fraction, *V* is the volume of the scatterer, *r* is the radius of the sphere and *background* is the background level. *sld* and *sld_solvent* are the scattering length densities (SLDs) of the scatterer and the solvent respectively, whose difference is $\Delta\rho$.

Table S1: SAXS fitting parameters for models based on three peaks

Composition	***x* = 0**	***x* = 1**
scale	1	1
peak1 scale	0.201	0.108
peak1 position (Å^{-1})	0.347	0.32
peak1 width (Å^{-1})	0.154	0.072
peak2 scale	0.125	0.21
peak2 position (Å^{-1})	0.53	0.52
peak2 width (Å^{-1})	0.5	0.472
peak3 scale	0.45	0.456
peak3 position (Å^{-1})	1.47	1.185
peak3 width (Å^{-1})	0.37	0.252

Table S2 SAXS fitting parameters for model based on three peaks and a spherical form factor

Composition	***x* = 0.1**	***x* = 0.2**	***x* = 0.3**	***x* = 0.4**	***x* = 0.5**	***x* = 0.6**	***x* = 0.7**	***x* = 0.8**	***x* = 0.9**
scale	1	1	1	1	1	1	1	1	1
sphere scale	0.116	0.181	0.282	0.19	0.15	0.15	0.067	0.049	0.02
sphere radius (Å)	10.25	10	9.8	9.8	9.8	9.8	9.65	9.65	9.65
peak1 scale	0.276	0.342	0.37	0.293	0.268	0.254	0.176	0.153	0.139
peak1 position (Å^{-1})	0.335	0.31	0.28	0.265	0.27	0.28	0.3	0.31	0.31
peak1 width (Å^{-1})	0.188	0.273	0.231	0.13	0.144	0.115	0.1	0.09	0.088
peak2 scale	0.283	0.088	0.147	0.308	0.217	0.244	0.23	0.243	0.179
peak2 position (Å^{-1})	0.45	0.45	0.45	0.37	0.4	0.4	0.45	0.47	0.5
peak2 width (Å^{-1})	0.581	0.5	0.5	0.489	0.479	0.459	0.48	0.496	0.446
peak3 scale	0.592	0.351	0.339	0.392	0.372	0.396	0.405	0.439	0.43
peak3 position (Å^{-1})	1.43	1.36	1.272	1.22	1.215	1.208	1.195	1.195	1.185
peak3 width (Å^{-1})	0.427	0.386	0.319	0.298	0.266	0.271	0.258	0.266	0.247

Table S3: SANS fitting parameters for model based on three peaks

Composition	***x* = 0**
scale	1
peak1 scale	0.107
peak1 position (Å^{-1})	0.365
peak1 width (Å^{-1})	0.119
peak2 scale	0.117
peak2 position (Å^{-1})	0.53
peak2 width (Å^{-1})	0.241
peak3 scale	0.28
peak3 position (Å^{-1})	1.47
peak3 width (Å^{-1})	0.35

Table S4: SANS fitting parameters for model based on three peaks and a Lorentzian function centred at q = 0

Composition	***x* = 1**
scale	1
Lorentz scale	0.096
Corr length (Å)	12
peak1 scale	0.114
peak1 position (Å^{-1})	0.305
peak1 width (Å^{-1})	0.074
peak2 scale	0.049
peak2 position (Å^{-1})	0.47
peak2 width (Å^{-1})	0.22
peak3 scale	0.296
peak3 position (Å^{-1})	1.185
peak3 width (Å^{-1})	0.35

Table S5: SANS fitting parameters for model based on three peaks and a spherical form factor

Composition	***x* = 0.1**	***x* = 0.2**	***x* = 0.3**	***x* = 0.4**	***x* = 0.5**	***x* = 0.6**	***x* = 0.7**	***x* = 0.8**	***x* = 0.9**
scale	1	1	1	1	1	1	1	1	1
sphere scale	0.071	0.16	0.218	0.239	0.218	0.143	0.102	0.055	0.04
sphere radius (Å)	10.25	10.22	10.08	9.80	9.65	9.65	9.65	9.65	9.65
peak1 scale	0.194	0.272	0.324	0.371	0.339	0.3	0.307	0.234	0.151
peak1 position (Å^{-1})	0.36	0.34	0.31	0.275	0.26	0.27	0.285	0.295	0.297
peak1 width (Å^{-1})	0.192	0.251	0.282	0.312	0.235	0.18	0.142	0.121	0.094
peak2 scale	0.0437	0.0001	0.0001	0.0001	0.0317	0.039	0.109	0.099	0.07
peak2 position (Å^{-1})	0.53	0.53	0.53	0.53	0.53	0.53	0.53	0.53	0.51
peak2 width (Å^{-1})	0.3	0.25	0.25	0.25	0.25	0.25	0.25	0.25	0.23
peak3 scale	0.157	0.123	0.173	0.193	0.176	0.184	0.325	0.355	0.242
peak3 position (Å^{-1})	1.43	1.36	1.272	1.22	1.215	1.208	1.195	1.195	1.185
peak3 width (Å^{-1})	0.45	0.4	0.3	0.3	0.3	0.3	0.3	0.3	0.3

Table S6: Summary of SAXS fitting derived length scales

Composition	***x* = 0.1**	***x* = 0.2**	***x* = 0.3**	***x* = 0.4**	***x* = 0.5**	***x* = 0.6**	***x* = 0.7**	***x* = 0.8**	***x* = 0.9**	***x* = 0.1**	***x* = 1**
CP (Å)	4.27	4.39	4.62	4.94	5.15	5.17	5.20	5.26	5.26	5.30	5.30
CP est. error +/- (Å)	0.03	0.03	0.03	0.03	0.03	0.02	0.02	0.02	0.02	0.02	0.02
PNPP (Å)	18.1	18.8	20.3	22.4	23.7	23.3	22.4	20.9	20.3	20.3	19.6
PNPP est. error +/- (Å)	0.2	0.2	0.7	1.3	0.7	0.6	0.3	0.2	0.2	0.2	0.2
Sphere radius (Å)		10.3	10.0	9.8	9.8	9.8	9.8	9.7	9.7	9.7	

Table S7: Summary of SANS fitting derived lengthscales

Composition	***x* = 0.1**	***x* = 0.2**	***x* = 0.3**	***x* = 0.4**	***x* = 0.5**	***x* = 0.6**	***x* = 0.7**	***x* = 0.8**	***x* = 0.9**	***x* = 0.1**	***x* = 1**
CP (Å)	4.27	4.39	4.62	4.94	5.15	5.17	5.20	5.26	5.26	5.30	5.30
PNPP (Å)	17.2	17.5	18.5	20.3	22.8	24.2	23.3	22.0	21.3	21.2	20.6
PNPP est. error +/- (Å)	0.5	0.8	0.9	1.0	1.3	1.0	0.6	0.5	0.4	0.3	0.3
Sphere radius (Å)		10.3	10.2	10.1	9.8	9.7	9.7	9.7	9.7	9.7	

No estimated error for CP, as this peak is not clearly visible within the *q*-range of the SANS data. CP position fixed at the value determined in the SAXS fits.

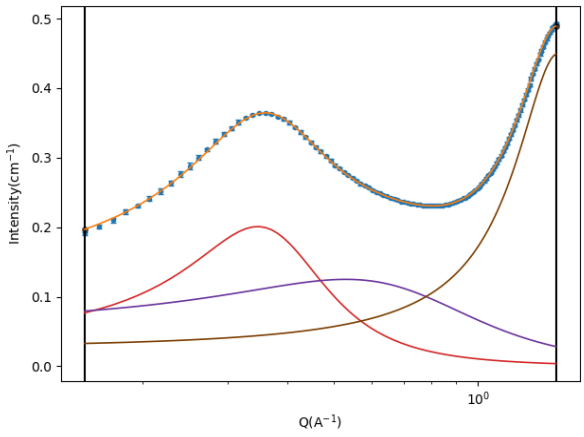

***x* = 0**

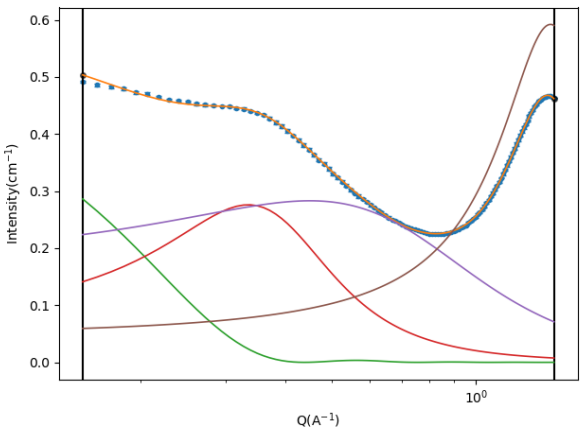

***x* = 0.1**

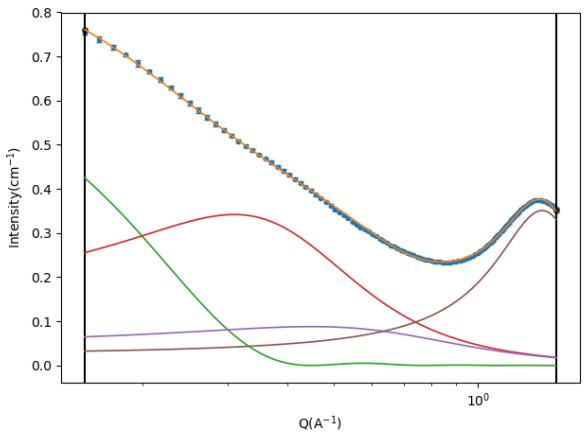

***x* = 0.2**

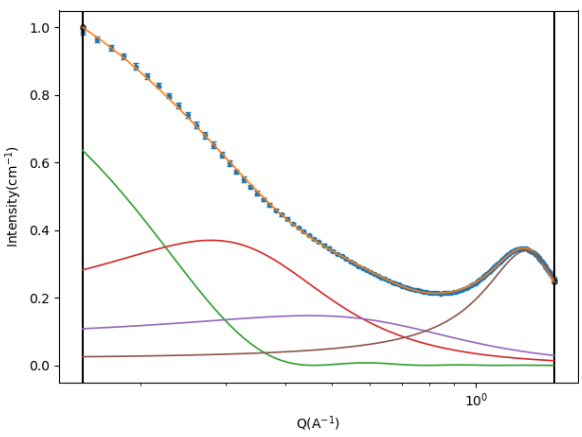

***x* = 0.3**

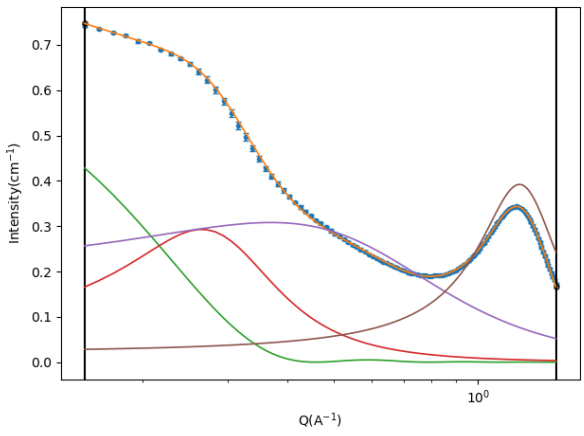

***x* = 0.4**

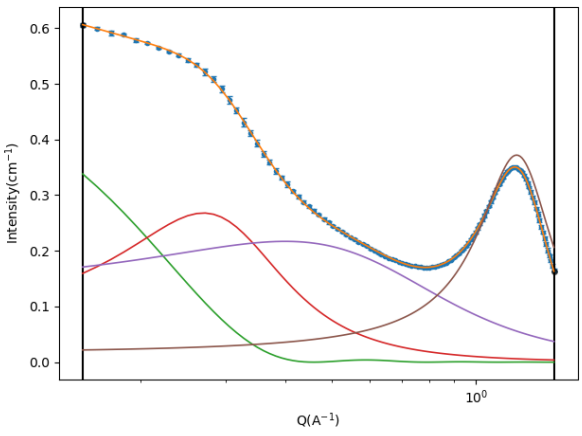

***x* = 0.5**

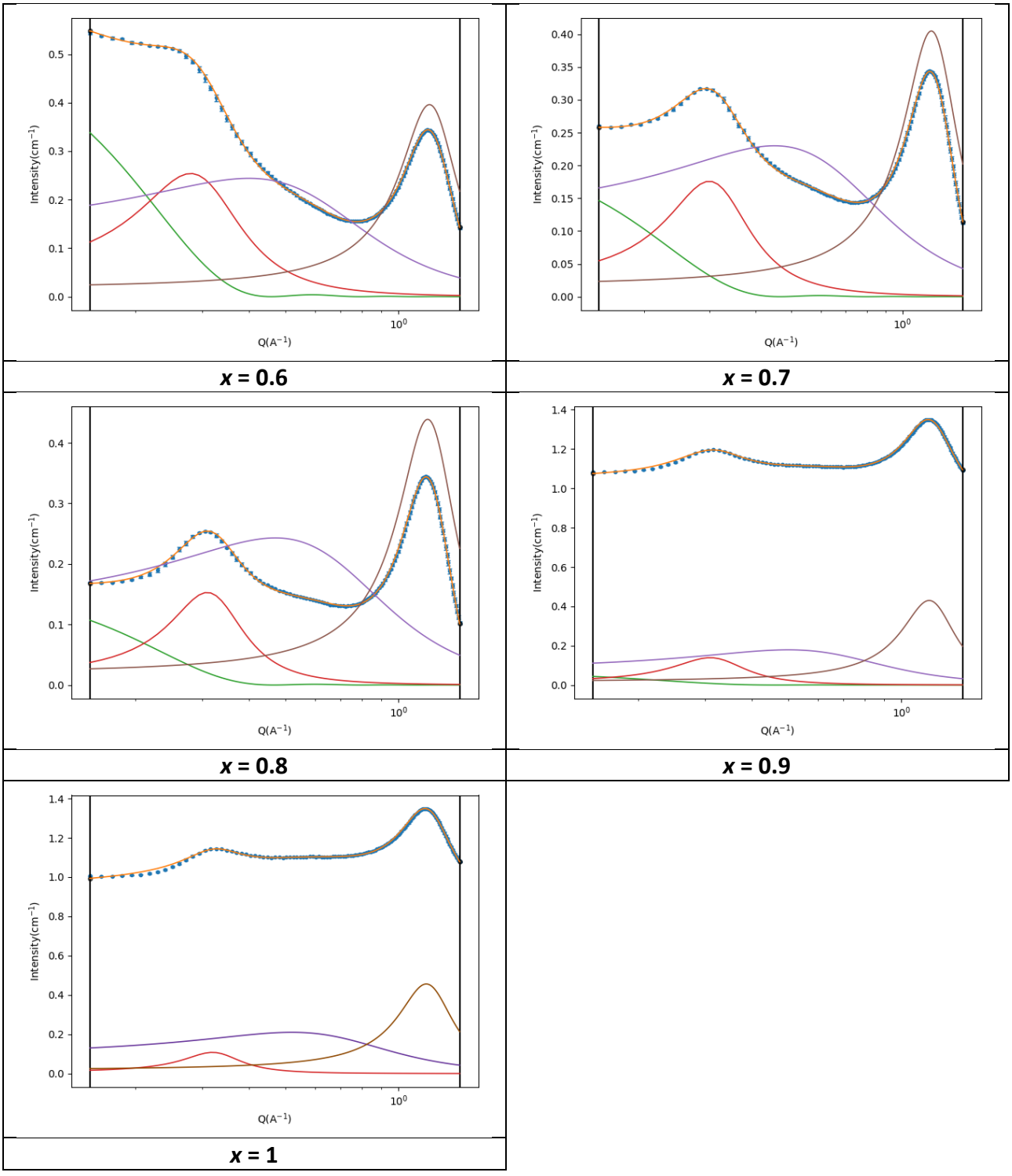

Figure S1: Plots of SAXS data fits. Orange: Overall fit. Green: Sphere. Red: PNPP. Brown: CP.

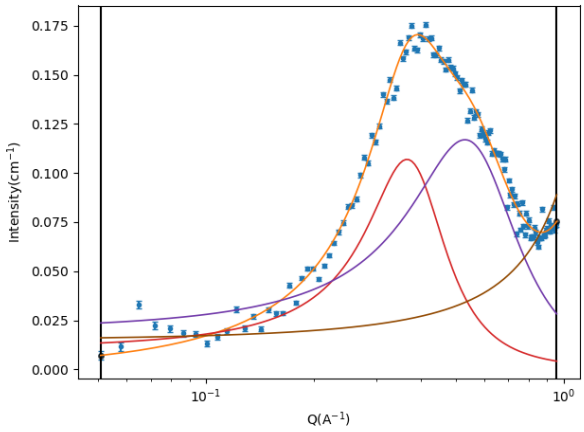

***x* = 0**

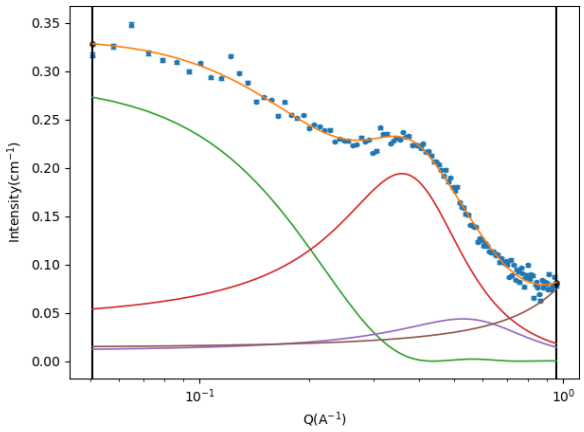

***x* = 0.1**

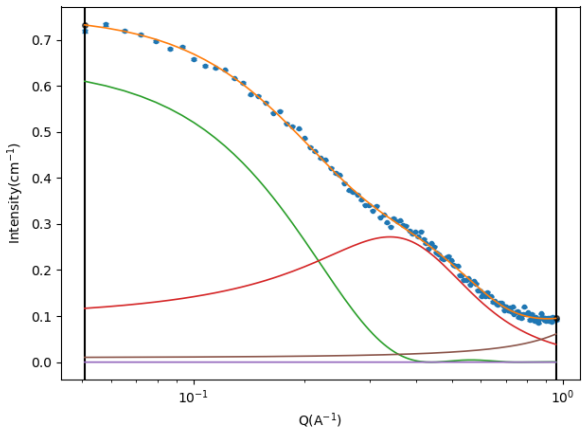

***x* = 0.2**

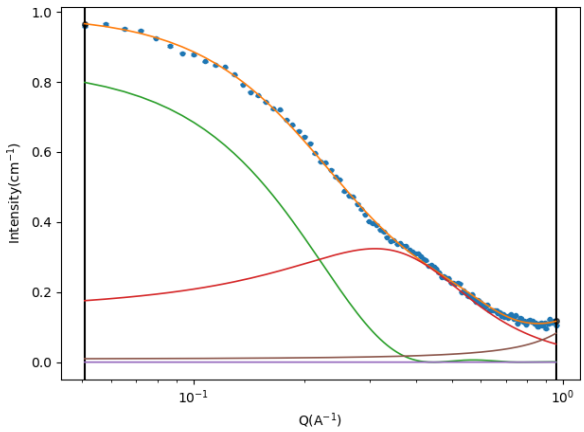

***x* = 0.3**

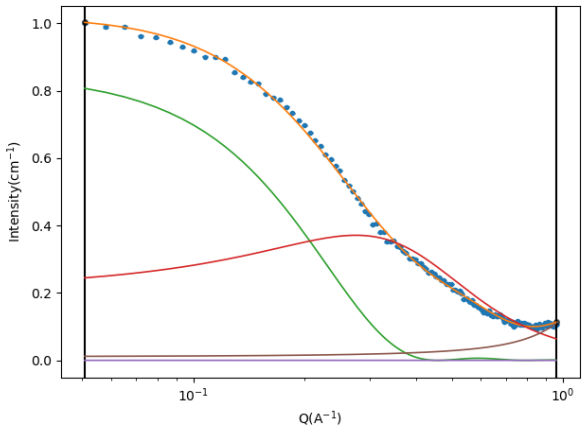

***x* = 0.4**

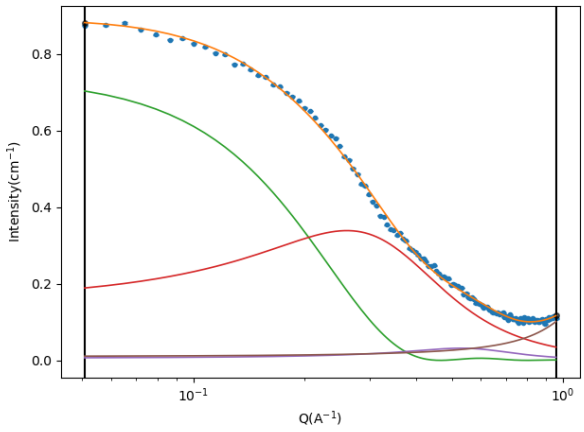

***x* = 0.5**

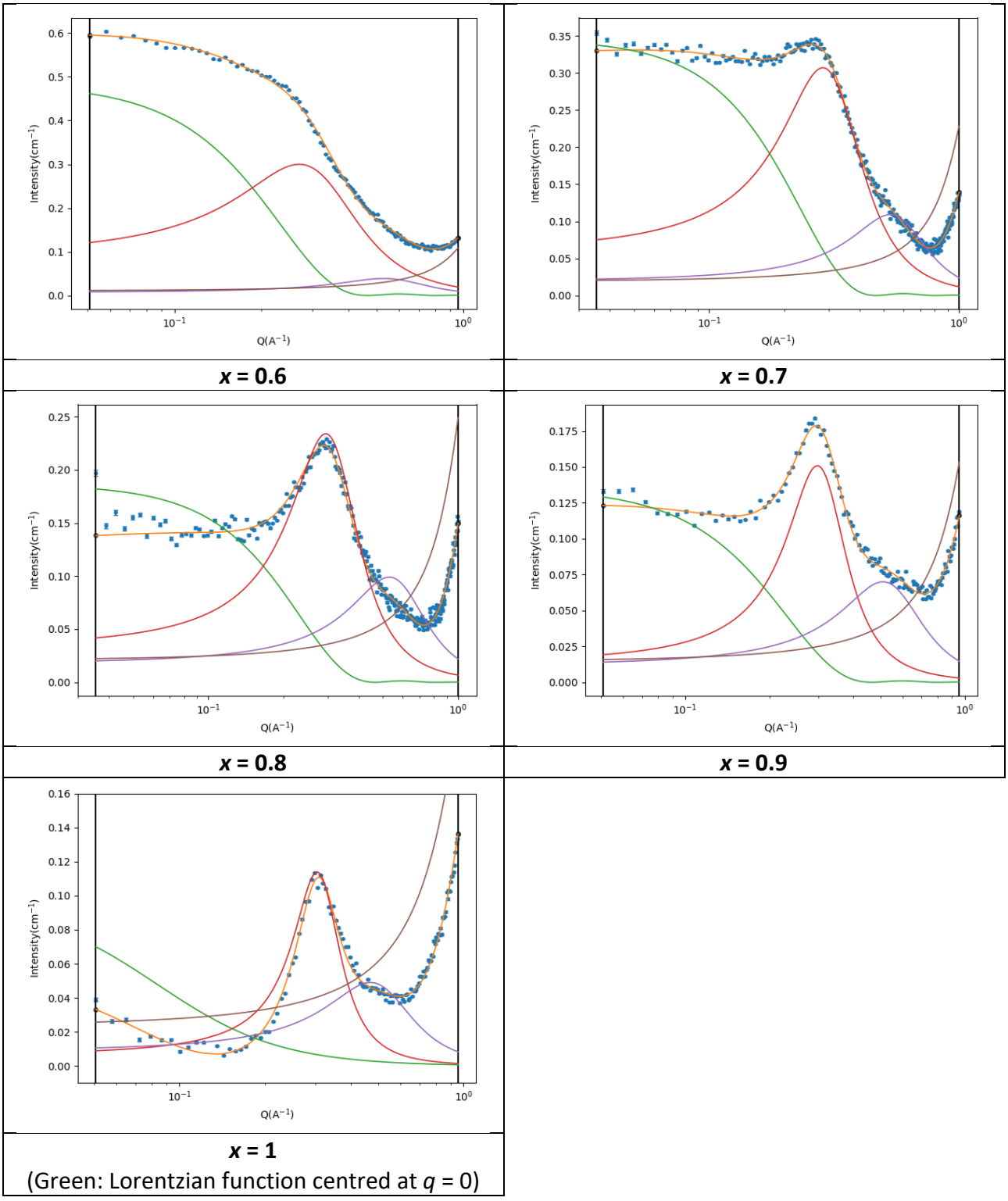

Figure S2: SANS fits Orange: Overall fit. Green: Sphere. Red: PNPP. Brown: CP.

Density Measurements

Density measurements used an Anton Paar DSA 5000 vibrating tube densitometer at 20 °C, calibrated according to the manufacturer's protocol and each data point was calculated from the average of multiple runs. The manufacturer's specification of accuracy in the measurements is ±1 μg cm^{-3} and their specified temperature accuracy is given as ±1 mK.

Molecular dynamics simulations

Molecular dynamics simulations were carried out using DL_POLY 2.20 and GROMACS 5.1.4 packages.[5-10] The mixtures were modelled using the OPLS/AMBER-like CL&P force field.[11,12] The scaling factor of α = 0.8 was applied to the partial charges of the charged part of the cation and the anion. The simulations started from low-density configurations with 2000 ion pairs built with fftool and Packmol software.[13,14] The runs were performed using 2 fs timesteps and 1.2 nm cut-off distances, followed by a 10 ns simulated annealing scheme. In the annealing process, the temperature ranges from 300 to 550 K, V-rescale thermostat and Berendsen barostat relaxation times of 0.5 and 4 ps, respectively, and then brought down to 300 K temperature and 1 atm pressure. These simulations were equilibrated under isobaric isothermal ensemble conditions (p = 0.1 MPa and T = 300 K, with V-rescale thermostat and Berendsen barostat relaxation time constants of 0.5 and 2 ps, respectively), using 2 fs timestep and 1.6 nm cut-off distance for 25 ns. The density of each system reached a constant and consistent value after 10 ns, indicating that equilibrium had been attained and possible ergodicity problems had been overcome. Finally, a 10 ns production stage was performed using 1 fs timestep in isothermal-isobaric ensemble conditions p = 0.1 MPa and T = 300 K, with Nosé−Hoover thermostat and Parrinello-Rahman barostat relaxation times of 0.5 and 4 ps, respectively. The final volumes of the simulation boxes were larger than 10 x 10 x 10 nm^3. Pair correlation functions, $g_{ij}(r)$, and total structure factor functions, $S(q)$, were calculated according to the formulas and methodologies described previously.[15]

Quantum Chemical Calculations

The geometries were optimised in Gaussian16 with CAM-B3LYP/6-311G(3df,3pd).[16,17] The vibrational frequencies were checked for true minima in all cases (no imaginary frequencies were found). Electrostatic charge distributions were calculated at the CAM-B3LYP/6-311G(3df,3pd) level of theory. The point charges placed at the centre of mass of each atom of the molecules are then calculated from the electronic density function using an electrostatic surface potential methodology (CHelpG).

Synthesis

As a general precaution, reactions were performed under an inert atmosphere of dinitrogen using standard Schlenk line techniques. Solvents were purchased as HPLC-grade reagents. Other chemicals purchased from Sigma-Aldrich were of puriss p.a., ACS reagent grade, and were used without further purification, unless stated otherwise. Sodium hydride (60% dispersion in paraffin oil) was separately purchased from TCI. Acetonitrile and tetrahydrofuran were purified with the aid of state-of-the-art PureSolv^{TM} solvent purification system. All bromoalkane reagents were freshly distilled over activated 3 Å molecular sieves under reduced pressure (10^{-3} torr) prior to use.

In the ^{1}H NMR spectra, there is some evidence of coupling between the imidazole hydrogen atoms that is partially resolved in the hydrogen atom adjacent to the unbound nitrogen, but is represented only by unresolved broadening in the other two. As such, all are recorded as singlets to avoid confusion.

The products are all purified by short-path, vacuum distillation ensuring a high degree of purity. Nonetheless, the imidazole group is polar and Karl Fischer titration for C_8Im shows some evidence of water (not measured for C_{10}Im as not ST data were recorded), consistent with deviations from expected CHN values in combustion analysis. Calculations shows *ca* 0.125 mol eq. of water in CHN data for both C_8Im and C_{10}Im.

Synthesis of 1-Octylimidazole, C_8Im

Imidazole (10 g, 146.88 mmol, 1.05 mol. eq.) was slowly added to a suspension of NaH (60% dispersion in paraffin oil, 1 mol. eq. of NaH) in THF (200 mL) at 0 °C under continuous stirring for 30 min. The mixture was left to stir at room temperature for additional 30 min under N_2 flow, after which 1-bromooctane (24.15 mL, 139.9 mmol, 1 mol. eq.) was added dropwise, and the solution was left stirring for 2 d under reflux. After cooling, the solution was filtered and washed with dichloromethane (400 mL) over a pad of celite (13.5 x 2 cm) and extracted with distilled H_2O (3 x 400 mL). The organic layer was separated, dried over magnesium sulfate, filtered and concentrated *in vacuo* to yield a pale-yellow oil. The product was then purified by short-path vacuum distillation (105-109 °C; 0.10(4) torr) to yield the product as a colourless oil (21.9 g, 121.56 mmol, 86.9%).

^{1}H NMR (400 MHz, $CDCl_3$) δ/ppm: 7.45 (s, 1H), 7.05 (s, 1H), 6.90 (s, 1H), 3.91 (t, J = 7.1 Hz, 2H), 1.80 – 1.73 (m, 2H), 1.34 – 1.23 (m, 12H), 0.86 (t, J = 7.1 Hz, 3H); ^{13}C{^{1}H} NMR (101 MHz, $CDCl_3$) δ/ppm: 137.15, 129.44, 118.83, 47.10, 31.78, 31.15, 29.15, 29.09, 26.61, 22.66, 14.13. Anal. Calcd for $C_{11}H_{20}N_2$: %C = 73.28, %H = 11.18, %N = 15.54. Found: %C = 72.41, %H = 11.81, %N = 16.34. H_2O Content (Karl Fischer): 1175.66 ppm

Synthesis of 1-Decylimidazole, C_{10}Im

Imidazole (1 g, 14.7 mmol, 1.05 mol. eq.) was slowly added to a suspension of NaH (60% dispersion in paraffin oil, 1 mol. eq. of NaH) in THF (20 mL) at 0 °C under continuous stirring for 30 min. The mixture was left to stir at room temperature for 30 min under N_2 flow, after which 1-bromododecane (2.9 mL, 14.0 mmol, 1 mol. eq.) was added dropwise, and the solution was left for 24 h under reflux. After cooling, the solution was filtered, washed over a pad of celite with dichloromethane (40 mL) and extracted with distilled H_2O (3 x 40 mL). The organic layer was then separated, washed with brine, dried over magnesium sulfate, concentrated under reduced

pressure and purified by short-path vacuum distillation (83-85 °C; 0.008(2) torr) to yield the product as a colourless oil (2.3 g, 2.872 mmol, 79%).

^{1}H NMR (400 MHz, $CDCl_3$) δ/ppm: 7.45 (s, 1H), 7.05 (s, 1H), 6.90 (s, 1H), 3.91 (t, *J* = 7.2 Hz, 2H), 1.80 – 1.73 (m, 2H), 1.28 – 1.25 (m, 14H), 0.87 (t, *J* = 7.0 Hz, 3H); ^{13}C{^{1}H} NMR (101 MHz, $CDCl_3$) δ/ppm: 137.14, 129.39, 118.86, 47.15, 31.93, 31.16, 29.56, 29.51, 29.34, 29.15, 26.63, 22.74, 14.19. Anal. Calcd for $C_{13}H_{24}N_2$: %C = 74.94, %H = 11.61, %N = 13.45. Found: %C = 74.24, %H = 11.66, %N = 14.10.

Synthesis of 1-(1*H*,1*H*,2*H*,2*H*-Tridecafluorooctyl)imidazole, C_8Im-F_{13}

Imidazole (10 g, 146.89 mmol, 2 equiv.) and 1*H*,1*H*,2*H*,2*H*-pentafluorooctyl iodide (18 mL, 73.44 mmol, 1 mol. eq.) were added to anhydrous MeCN (125 mL) under a N_2 atmosphere. The yellow mixture was then heated to 45 °C under vigorous stirring. Gradual progression of the reaction was followed by ^{19}F NMR spectroscopy. After 7 d, the mixture was cooled and washed with MeCN (3 x 20 mL), after which it was concentrated to dryness as a pale-yellow solid. The crude product was dissolved in dichloromethane (200 mL) and filtered for extraction with distilled H_2O (3 x 200 mL). Afterwards, the organic layer was dried over magnesium sulfate and reduced under vacuum to yield a yellowish solid. The coloured impurities were removed *in vacuo* and the product was purified by short-path vacuum distillation (78-81 °C; 0.04(1) torr) to yield a colourless, crystalline solid (9.2 g, 32.6%); m.pt.53 – 55 °C; ^{1}H NMR (400 MHz, $CDCl_3$) δ/ppm: 7.53 (s, 1H), 7.11 (s, 1H), 6.95 (s, 1H), 4.30 (t, *J* = 7.5 Hz, 2H), 2.60 (m, 2H); ^{19}F NMR (376 MHz, $CDCl_3$) δ/ppm: -80.63 (t, *J* = 10.0 Hz, 3F), -114.11 (m, 2F), -121.74 (s, 2F), -122.73 (s, 2F), -123.33 (s, 2F), -126.00 (m, 2F). Anal. Calcd for $C_{11}H_7F_{13}N_2$: %C = 31.90, %H = 1.70, %N = 6.76, %F = 59.63. Found: %C = 31.63, %H = 1.16, %N = 6.75, %F = 60.46. H_2O Content: 1918.97 ppm

Synthesis of 1-(1*H*,1*H*,2*H*,2*H*-Heptadecafluorodecyl)imidazole, C_{10}Im-F_{17}

Imidazole (1 g, 18.826 mmol, 1.05 mol. eq.) and 1*H*,1*H*,2*H*,2*H*-perfluorodecyl iodide (10.3 g, 17.93 mmol, 1 mol. eq.) were added into anhydrous MeCN (25 mL) under vigorous stirring under a N_2 flow. The mixture was gradually heated to 80 °C. After 6 d, the mixture was cooled to room temperature, filtered and washed with MeCN (3 x 20 mL), after which it was concentrated to dryness as a pale orange solid. The crude solid was dissolved in dichloromethane (40 mL) for extraction with distilled H_2O (3 x 40 mL). The organic layer was separated, washed with brine, dried over magnesium sulfate, and concentrated under reduced pressure to yield a yellow solid. The coloured impurities were removed *in vacuo* and the product was purified by short-path vacuum distillation (63-65 °C; 0.007(3) torr) to yield colourless, crystalline needles (0.95 g, 2.3 mmol, 10%); m.pt. 91 °C; ^{1}H NMR (400 MHz, $CDCl_3$) δ/ppm: 7.53 (s, 1H), 7.11 (s, 1H), 6.95 (s, 1H), 4.30 (t, *J* = 7.5 Hz, 2H), 2.59 (m, 2H); ^{19}F NMR (376 MHz, $CDCl_3$) δ/ppm: -80.61 (t, *J* = 10.1 Hz, 3F), -114.11 (m, 2F), -121.51 (s, 2F), -121.76 (m, 4F), -122.57 (s, 2F), -123.26 (s, 2F), -125.96 (m, 2F). Anal. Calcd for $C_{13}H_7F_{17}N_2$: %C = 30.37, %H = 1.37, %N = 5.45, %F = 62.81. Found: %C = 30.53, %H = 1.29, %N = 6.1, %F = 61.97.

Preparation of Mixtures

Samples of pure C_8Im and C_8Im-F_{13} were mixed to prepare the non-ionic surfactant mixtures of $[C_8Im]_{(1-x)}[C_8Im\text{-}F_{13}]_x$, where x = 0.1 – 0.9, at 296 K under atmospheric pressure, using an analytical balance, Mettler Toledo XPR XS105, with a resolution of ± 0.01 mg. All molar compositions were prepared up to a total sample volume of 1 mL, which require mass-to-volume conversions by their density over a mass range of 0.1 – 1.6 g. Homogenisation was ensured *via* a Cole-Parmer Stuart vortex mixer and a sonication bath for about 30 min at 333 K, resulting in a total of nine colourless mixtures. The mixtures were then allowed to equilibrate at 333 K, and stored in the dark at 293 ± 2 K.

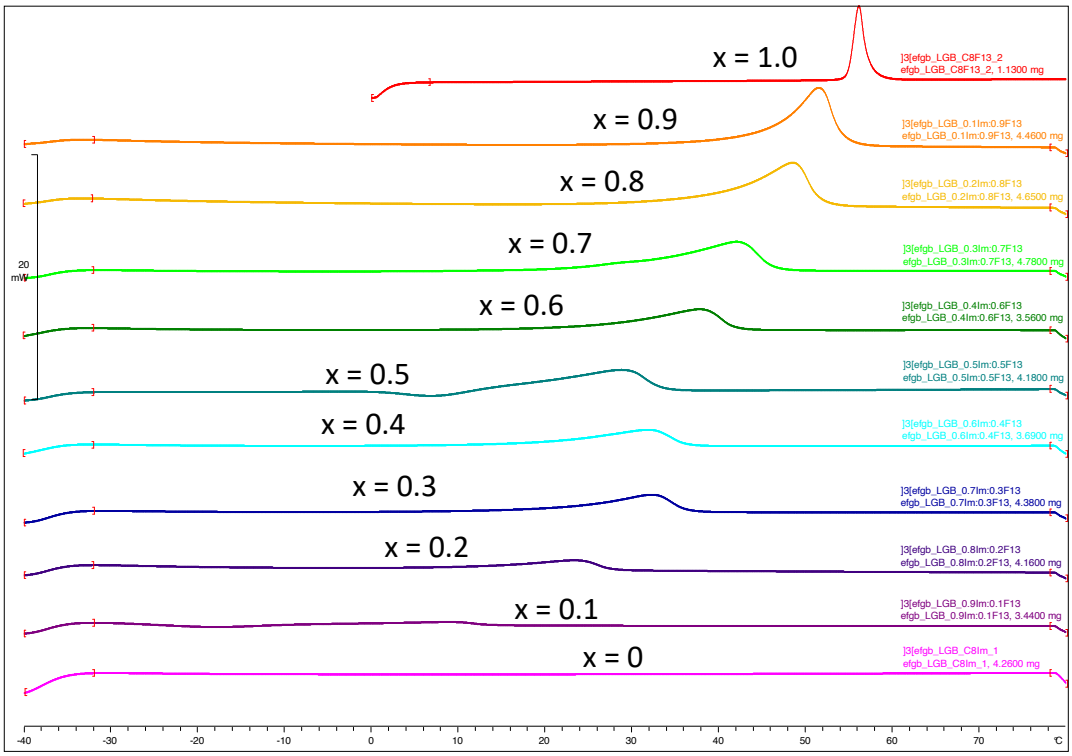

T / °C

Figure S3 DSC heating traces for the mixtures $[C_8Im]_{1-x}[C_8Im\text{-}F_{13}]_x$.

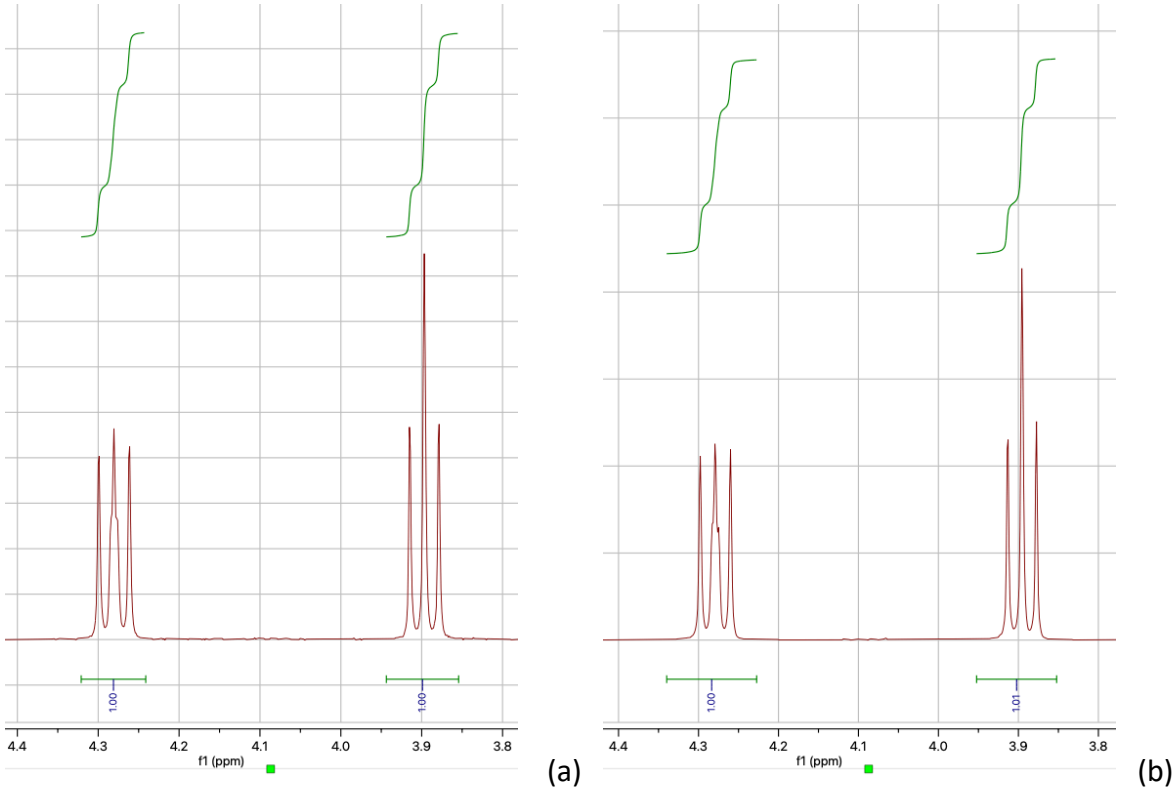

Figure S4 Integration of the N-CH_2 hydrogens in a 1:1 mixture of C_8Im and C_8Im-F_{13} taken from (a) the top and (b) the bottom of a sample that had been allowed to equilibrate undisturbed at 60 °C for a month. The N-CH_2 hydrogens from C_8Im are at *ca* 3.9 ppm, while those from C_8Im-F_{13} are found at *ca* 4.3 ppm.

Determination of the Density of C_8Im-F_{13}

Previous work had shown that for two related components of equal chain length, the variation of density with composition was linear. For the mixtures $[C_8Im]_{1-x}[C_8Im\text{-}F_{13}]_x$, most were solids at room temperature, but for x = 0.05, 0.1 and 0.15 the mixtures were liquid and so the density was measured for these compositions. The data are plotted below in Fig. S6 and the line can be extrapolated to x = 1 where the density is calculated to be 1.75 g cm^{-3} (line R-factor = 0.9999).

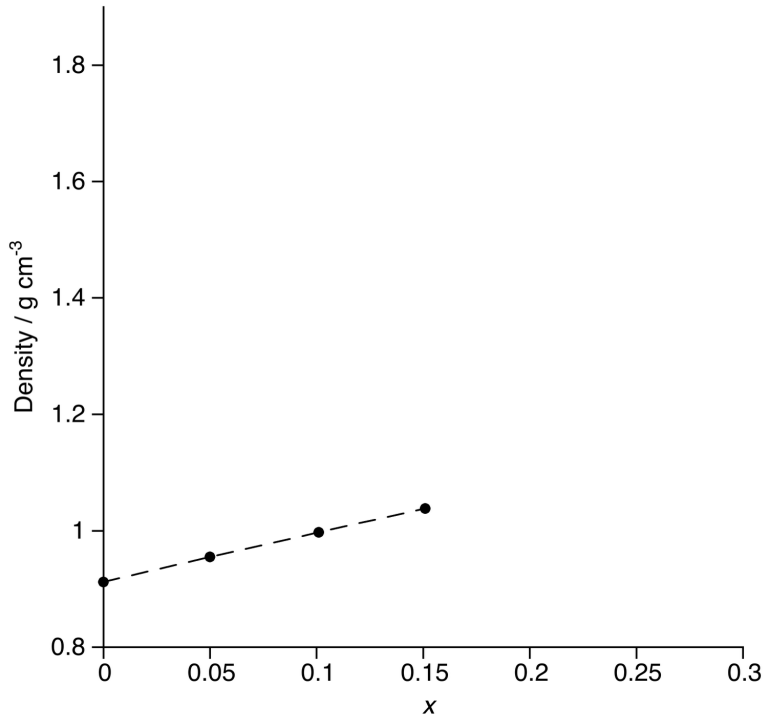

Figure S5 Experimental density data for $[C_8Im]_{1-x}[C_8Im\text{-}F_{13}]_x$ over compositions where the mixture is fluid at ambient temperature.

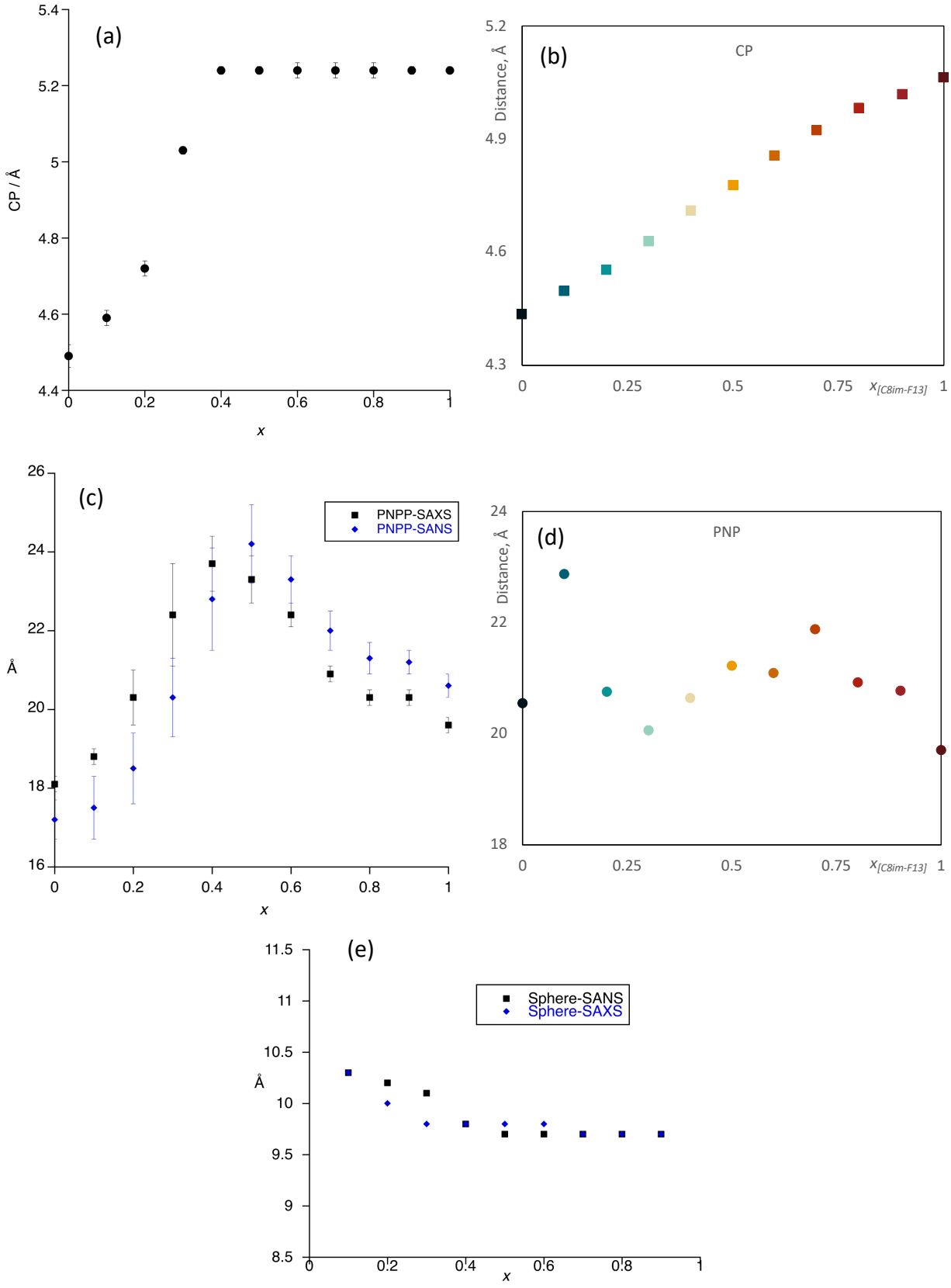

Figure S6 Evolution as a function of composition of the CP (a) from SAXS data and (b)from MD calculations; evolution of the PNPP (c) from scattering data and (d) from MD calculations; (e) sphere radius (from SANS data).

Variation of the SLD Contrast with Composition

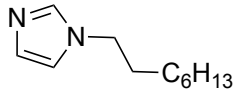

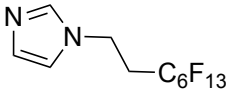

Contrast in the two components is derived from the magnitude of the difference between the imidazole plus two CH_2 groups (1.37×10^{-6} Å^{-2}) and either the C_6H_{13} chain (-0.576×10^{-6} Å^{-2}) or the C_6F_{13} chain (3.54×10^{-6} Å^{-2}). These are 1.946×10^{-6} Å^{-2} (C_8Im) and 2.17×10^{-6} Å^{-2} (C_8Im-F_{13}). While it is understood that the contrast is proportional to the square of the SLD difference, as it is a null point that is being sought, the it is simpler to plot as a linear function, as shown in Fig. S8, showing that the contrast giving rise to the PNPP is lost at x = 0.47 in the mixtures $[C_8Im]_{1-x}[C_8Im\text{-}F_{13}]_x$.

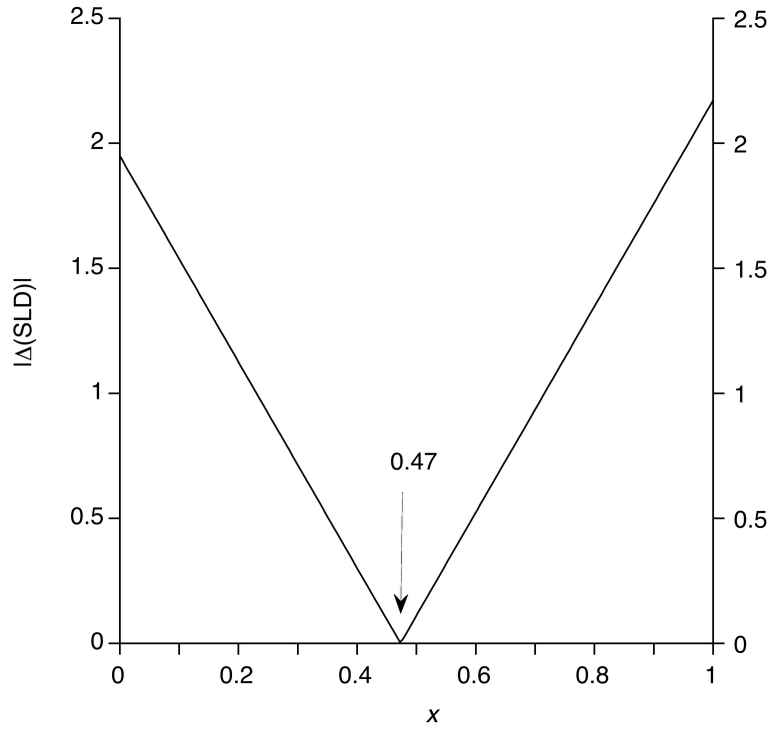

Figure S7 Variation of the (linear) SLD difference between headgroup and chain as a function of composition for $[C_8Im]_{1-x}[C_8Im\text{-}F_{13}]_x$.

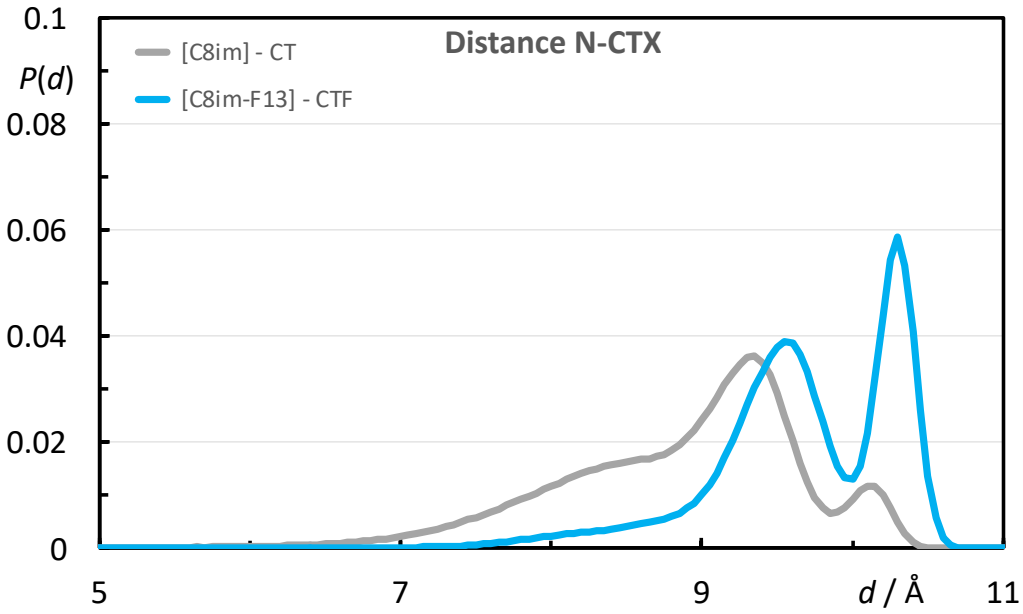

Figure S8 Plot of the probability $P(d)$ of finding a separation d between the terminal carbon atom in the chain and the unbound nitrogen in the imidazole ring.

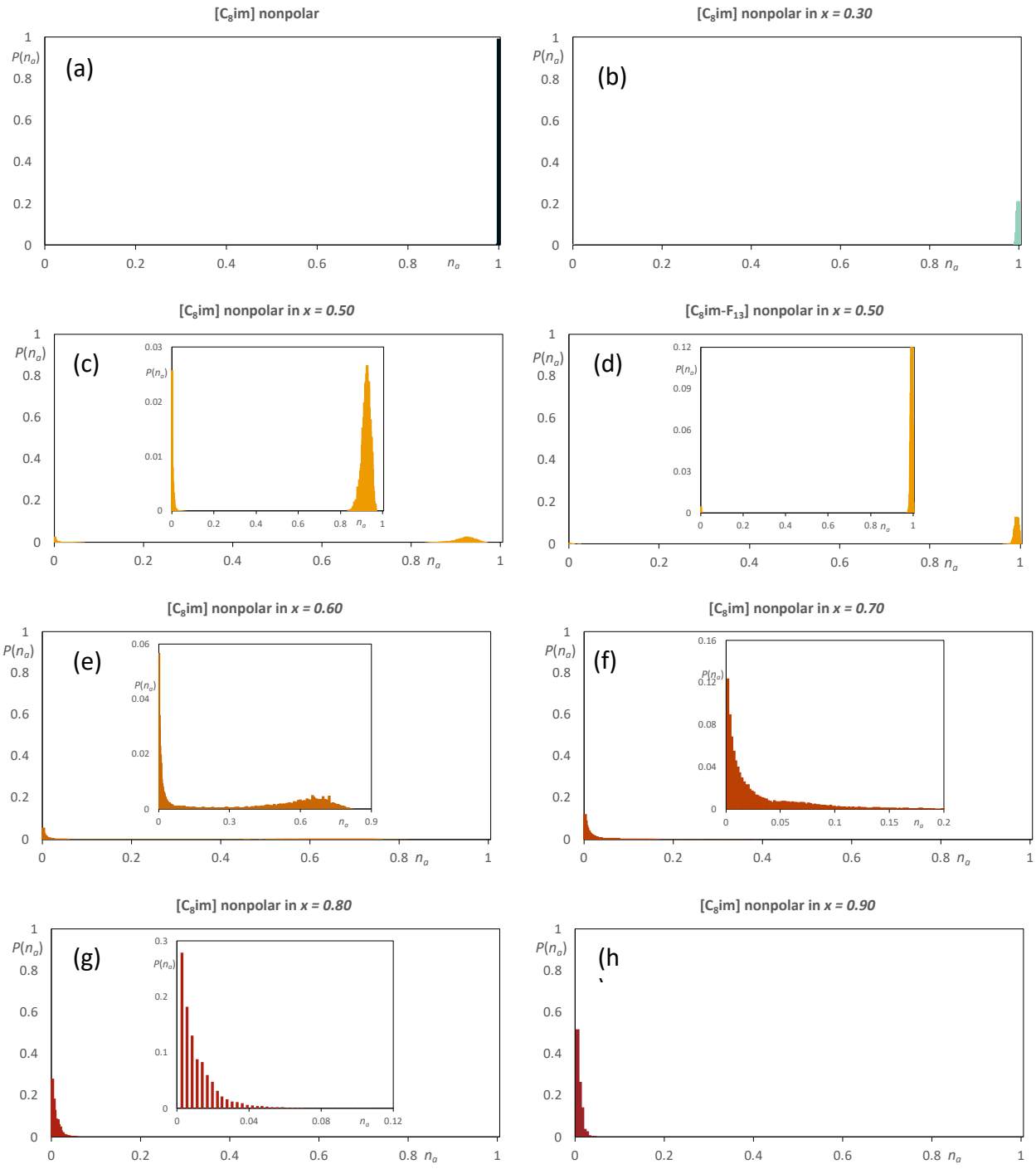

Figure S9 Discrete probability distribution function, $P(n_a)$, for the hydrocarbon chains in C_8Im belonging to a non-polar aggregate in the mixtures $[C_8Im]_{1-x}[C_8Im\text{-}F_{13}]_x$ for: (a) x = 0 and (b) x = 0.3. Discrete probability distribution function, $P(n_a)$, for the hydrocarbon chains in C_8Im and for the fluorous chains of C_8Im-F_{13} belonging to a non-polar aggregate in the mixtures $[C_8Im]_{1-x}[C_8Im\text{-}F_{13}]_x$ for: (c) & (d) x = 0.5; (e) & (f) x = 0.7 and (g) & (h) x = 0.0.

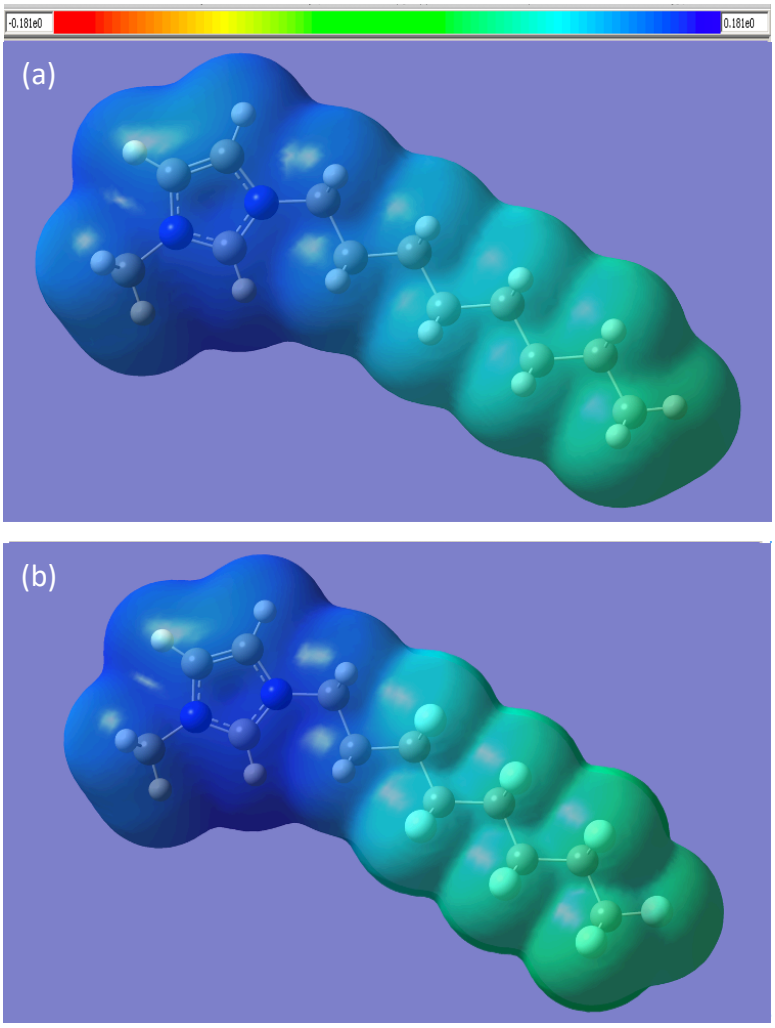

Figure S10 Electrostatic surface potential (the functional employed is CAM-B3LYP with the 6-311G(3df,3pd) basis set) for the cations (a) $[C_8MIM]^+$ and (b) $[C_8MIM\text{-}F_{13}]^+$ at an isosurface of 181 e $Å^3$.

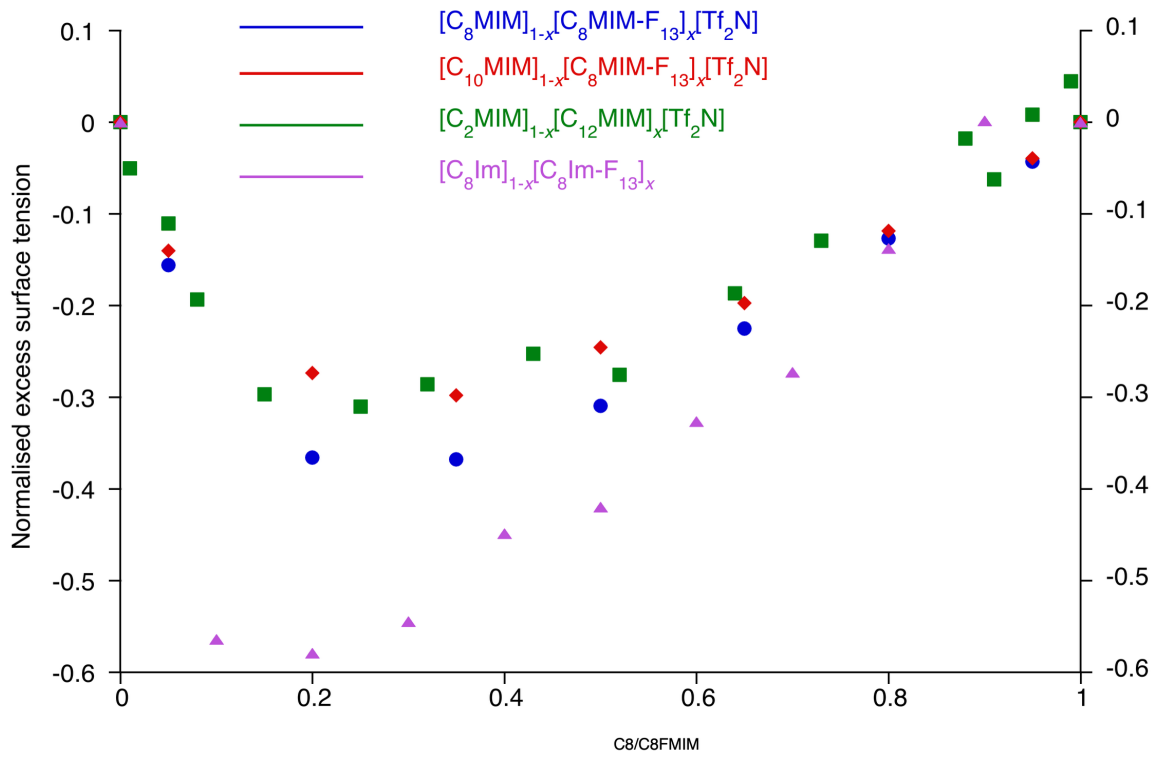

Figure S11 Excess surface tension for the mixtures $[C_8Im]_{1-x}[C_8Im\text{-}F_{13}]_x$, $[C_8MIM]_{1-x}[C_8MIM\text{-}F_{13}]_x[Tf_2N]$, $[C_{10}MIM]_{1-x}[C_8MIM\text{-}F_{13}]_x[Tf_2N]$ and $[C_2MIM]_{1-x}[C_{12}MIM]_x[Tf_2N]$, normalised for the total change in surface tension between the two components in each mixture.

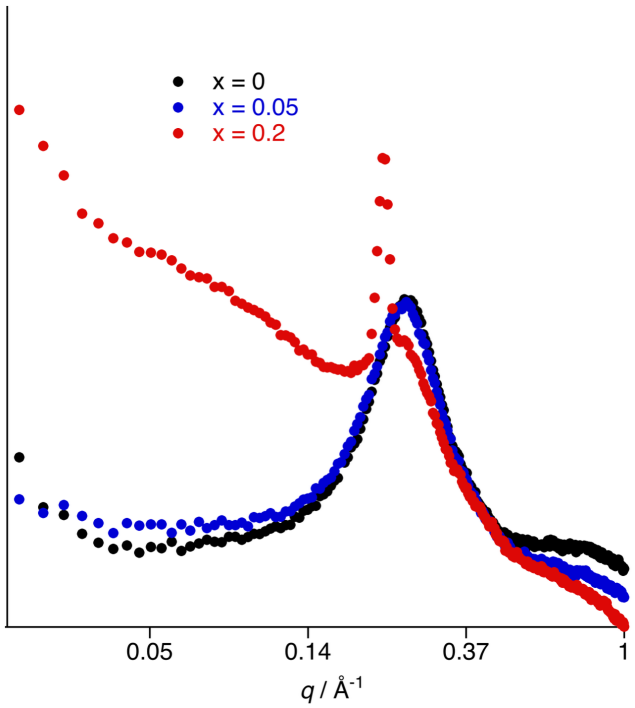

Figure S12 SANS data for the mixtures $[C_{12}MIM]_{1-x}[C_{12}MIM\text{-}F_{21}]_x[Tf_2N]$ for x = 0.0, 0.05 and 0.2.

References

1. H. Kou, W. Li, X. Zhang, N. Xu, X. Zhang, J. Shao, Y. Deng and Y. Li, *Fluid Phase Equil.*, 2019, **484**, 53-59.
2. J.-C. Buffet, V. Cristiglio, S. Cuccaro, B. Demé, B. Guérard, J. Marchal, J. Pentenero, N. Sartor and J. Turi, *EPJ Web of Conferences*, 2023, **286**, 03010.
3. O. Arnold, J. C. Bilheux, J. M. Borreguero, A. Buts, S. I. Campbell, L. Chapon, M. Doucet, N. Draper , R. Ferraz Leal, M. A. Gigg, V. E. Lynch, A. Markvardsen, D. J. Mikkelson, R. L. Mikkelson, R. Miller, K. Palmen, P. Parker, G. Passos, T. G. Perring, P. F. Peterson, S. Ren, M. A. Reuter, A. T. Savici, J. W. Taylor, R. J. Taylor, R. Tolchenov, W. Zho, J. Zikovsky, *Nucl. Instruments Methods Phys. Res. Sect. A Accel. Spectrometers, Detect. Assoc. Equip.*, 2014, **764**, 156–166.
4. A. Guinier and G. Fournet, *Small-Angle Scattering of X-Rays*, Wiley, New York, 1955.
5. W. Smith and T. R. Forester, The DL_POLY Package of Molecular Simulation Routines, (2006).
6. H. Bekker, H. Berendsen, E. Dijkstra, S. Achterop, R. Van Drunen, D. Van der Spoel, A. Sijbers, H. Keegstra, B. Reitsma and M. Renardus, *GROMACS: A Parallel Computer for Molecular Dynamics Simulations*, in: *Proc. 4th Int. Conf. Phys. Comput.*, 1993: pp. 252–256.
7. H. Berendsen, D. Van der Spoel and R. Van Drunen, *Comput. Phys. Commun.,* 1995, **91** 43–56.
8. D. Van Der Spoel, E. Lindahl, B. Hess, G. Groenhof, A. E. Mark and H. J. C. Berendsen, *J. Comput. Chem.*, 2005, **26**, 1701–1718.
9. S. Páll, M. J. Abraham, C. Kutzner, B. Hess and E. Lindahl, *Tackling Exascale Software Challenges in Molecular Dynamics Simulations with GROMACS*, in: *Proc. EASC 2015 LNCS*, 2015: pp. 3–27.
10. M. J. Abraham, T. Murtola, R. Schulz, S. Páll, J. C. Smith, B. Hess and E. Lindahl, *SoftwareX.*, 2015, **1–2**, 19–25.
11. W. L. Jorgensen, D. S. Maxwell and J. Tirado-Rives, *J. Am. Chem. Soc.*, 1996, **118**, 11225–11236.
12. J. N. Canongia Lopes and A. A. H. Pádua, *Theor. Chem. Acc.*, 2012, **131**, 1129.
13. L. Martínez, R. Andrade, E. G. Birgin and J. M. Martínez, *J. Comput. Chem. 2*, 2009, **30**, 2157–2164.
14. A. Padua, K. Goloviznina, Z. Gong, agiliopadua/fftool: XML force field files (v1.2.1). Zenodo. https://doi.org/10.5281/zenodo.4701065, 2021. Accessed 08/05/2025.

15. N. S. Elstone, K. Shimizu, E. V. Shaw, P. D. Lane, L. D'Andrea, B. Demé, N. Mahmoudi, S. E. Rogers, S. Youngs, M. L. Costen, K. G. McKendrick, J. N. Canongia Lopes, D. W. Bruce and J. M. Slattery, *J. Phys. Chem. B*, 2023, **127**, 7394-7407.
16. Gaussian 16, Revision A.03, M. J. Frisch, G. W. Trucks, H. B. Schlegel, G. E. Scuseria, M. A. Robb, J. R. Cheeseman, G. Scalmani, V. Barone, G. A. Petersson, H. Nakatsuji, X. Li, M. Caricato, A. V. Marenich, J. Bloino, B. G. Janesko, R. Gomperts, B. Mennucci, H. P. Hratchian, J. V. Ortiz, A. F. Izmaylov, J. L. Sonnenberg, D. Williams-Young, F. Ding, F. Lipparini, F. Egidi, J. Goings, B. Peng, A. Petrone, T. Henderson, D. Ranasinghe, V. G. Zakrzewski, J. Gao, N. Rega, G. Zheng, W. Liang, M. Hada, M. Ehara, K. Toyota, R. Fukuda, J. Hasegawa, M. Ishida, T. Nakajima, Y. Honda, O. Kitao, H. Nakai, T. Vreven, K. Throssell, J. A. Montgomery, Jr., J. E. Peralta, F. Ogliaro, M. J. Bearpark, J. J. Heyd, E. N. Brothers, K. N. Kudin, V. N. Staroverov, T. A. Keith, R. Kobayashi, J. Normand, K. Raghavachari, A. P. Rendell, J. C. Burant, S. S. Iyengar, J. Tomasi, M. Cossi, J. M. Millam, M. Klene, C. Adamo, R. Cammi, J. W. Ochterski, R. L. Martin, K. Morokuma, O. Farkas, J. B. Foresman, and D. J. Fox, Gaussian, Inc., Wallingford CT, 2016.
17. T. Yanai, D. Tew and N. Handy, *Chem. Phys. Lett.* 2004, **393**, 51–57.